Published in final edited form as:
Clin Cancer Res. 2013 December 1; 19(23): . doi:10.1158/1078-0432.CCR-13-1305.

Targeting Src and tubulin in mucinous ovarian carcinoma

Tao Liu[1,2], **Wei Hu**[1], **Heather J. Dalton**[1], **Hyun Jin Choi**[1], **Jie Huang**[1], **Yu Kang**[1,3], **Sunila Pradeep**[1], **Takahito Miyake**[1], **Jian H. Song**[4], **Yunfei Wen**[1], **Chunhua Lu**[1], **Chad V. Pecot**[5], **Justin Bottsford-Miller**[1], **Behrouz Zand**[1], **Nicholas B Jennings**[1], **Cristina Ivan**[1,6], **Gary E. Gallick**[4], **Keith A Baggerly**[7], **David G. Hangauer**[8], **Robert L. Coleman**[1], **Michael Frumovitz**[1], and **Anil K. Sood**[1,6,9,*]

[1]Department of Gynecologic Oncology and Reproductive Medicine, The University of Texas MD Anderson Cancer Center, Houston, TX 77030, USA

[2]Department of General Surgery, Union Hospital, Tongji Medical College, Huazhong University of Science and Technology, Wuhan, Hubei 430022, P.R. China

[3]Department of Gynecology, Obstetrics and Gynecology, Hospital of Fudan University, Shanghai 20001, P.R. China

[4]Department of Genitourinary Medical Oncology, The University of Texas MD Anderson Cancer Center, Houston, TX 77030, USA

[5]Division of Cancer Medicine, The University of Texas MD Anderson Cancer Center, Houston, TX 77030, USA

[6]Center for RNA Interference and Non-Coding RNA, The University of Texas MD Anderson Cancer Center, Houston, TX 77030, USA

[7]Department of Bioinformatics and Computational Biology, The University of Texas MD Anderson Cancer Center, Houston, TX 77030, USA

[8]Kinex Pharmaceuticals LLC, New York State Center of Excellence in Bioinformatics and Life Sciences, Buffalo, NY 14203, USA

[9]Department of Cancer Biology, The University of Texas MD Anderson Cancer Center, Houston, TX 77030, USA

Abstract

Purpose—To investigate the antitumor effects of targeting Src and tubulin in mucinous ovarian carcinoma.

Experimental design—The *in vitro* and *in vivo* effects and molecular mechanisms of KX-01, which inhibits Src pathway and tubulin polymerization, were examined in mucinous ovarian cancer models.

Results—*In vitro* studies using RMUG-S and RMUG-L cell lines showed that KX-01 inhibited cell proliferation, induced apoptosis, arrested the cell cycle at the G2/M phase, and enhanced the cytotoxicity of oxaliplatin in the KX-01-sensitive cell line, RMUG-S. *In vivo* studies showed that KX-01 significantly decreased tumor burden in RMUG-S and RMUG-L mouse models relative to untreated controls, and the effects were greater when KX-01 was combined with oxaliplatin.

Correspondence: Anil K. Sood, Professor, Departments of Gynecologic Oncology and Cancer Biology, Unit 1362, The University of Texas MD Anderson Cancer Center, 1515 Holcombe Blvd, Houston, TX 77030, USA; phone: 713-745-5266; fax: 713-792-7586; asood@mdanderson.org.

Conflicts of interest: none to report

KX-01 alone and in combination with oxaliplatin significantly inhibited tumor growth by reducing cell proliferation and inducing apoptosis in vivo. *PTEN* knock-in experiments in RMUG-L cells showed improved response to KX-01. Reverse phase protein array analysis showed that in addition to blocking downstream molecules of Src family kinases, KX-01 also activated acute stress-inducing molecules.

Conclusion—Our results showed that targeting both the Src pathway and tubulin with KX-01 significantly inhibited tumor growth in preclinical mucinous ovarian cancer models, suggesting that this may be a promising therapeutic approach for patients with mucinous ovarian carcinoma.

Keywords

Ovarian carcinoma; Mucinous; Src kinase; Tubulin; KX-01

INTRODUCTION

Mucinous ovarian carcinoma is a relatively rare subset of ovarian cancer, accounting for 2–10% of all subtypes of epithelial ovarian cancer (1–2). While standard therapy for ovarian cancer includes taxane and platinum-based chemotherapy (3–4), such therapy is largely ineffective in patients with mucinous ovarian carcinoma. Consequently, the outcome of women with mucinous ovarian carcinoma is poorer than patients with other epithelial ovarian cancers (5–8). Novel therapeutic approaches are urgently needed to improve outcomes of patients with mucinous ovarian carcinoma.

The Src family of non-receptor protein tyrosine kinases (SFKs) regulates various aspects of tumor progression via multiple signaling pathways, including cell survival (PI3K/Akt), growth (Ras/MEK/ERK), metastasis (FAK/paxillin), and angiogenesis (STAT3/VEGF) (9). Increased Src activity has been demonstrated in colorectal, pancreatic, lung, breast, ovarian, and prostate carcinomas, highlighting Src as a potential therapeutic target (10–11). Preclinical data have demonstrated the antitumor activity of Src inhibitors in prostate, colon, and breast cancers (12–14). Recently, we reported that Src kinase is overexpressed in mucinous ovarian carcinoma (15). Several agents targeting Src, including dasatinib (BMS-354825; Bristol-Myers Squibb, New York, NY), saracatinib (AZD0530; AstraZeneca, Wilmington, DE), and bosutinib (SKI-606; Wyeth/Pfizer, New York, NY) are currently in clinical trials for the treatment of various solid tumors. However, monotherapy with a Src inhibitor shows little activity in unselected solid tumor patients (16), emphasizing the need for multi-targeted inhibitors and biomarker-driven studies.

KX-01 (Kinex Pharmaceuticals, Buffalo, NY) is a novel Src signaling inhibitor that, unlike other Src inhibitors, does not bind to the ATP site (17). In addition, KX-01 binds to a novel site on the tubulin heterodimer, resulting in inhibition of microtubule polymerization and broader antitumor activity (18). In this study, we evaluated the preclinical activity of KX-01 in mucinous ovarian carcinoma.

MATERIALS AND METHODS

Cell lines and culture

The derivation and source of RMUG-S and RMUG-L cell lines has been previously described (15). YDOV-151 (a kind gift from Dr. Kwong K. Wong, Department of Gynecologic Oncology and Reproductive Medicine, The University of Texas MD Anderson Cancer Center) and EFO-27 (a kind gift from Dr. Gordon Mills, Department of Systems Biology, MD Anderson Cancer Center) cell lines were originally isolated from women with mucinous ovarian carcinoma (19–20). Cell lines were maintained and propagated in

RPMI-1640 medium supplemented with 10% fetal bovine serum and 0.1% gentamicin sulfate (Gemini Bioproducts, Calabasas, CA). Clear cell ovarian cancer cell lines (ES-2 and TOV21G) were purchased from ATCC, and were maintained in specific medium as described previously (15, 21). Cell lines were characterized by the Cell Line Core Facility at MD Anderson, which provides authenticated cell lines. All cell lines were routinely tested to confirm the absence of *Mycoplasma*and all experiments were performed with cell lines at 60–80% confluence.

Reagents and antibodies

KX-01 was provided by Kinex Pharmaceuticals in water soluble powder form (KX-01: methanesulfonic acid salt). Oxaliplatin (Wyeth/Pfizer, New York, NY) and paclitaxel (Bristol-Myers Squibb, New York, NY) were purchased from the institutional pharmacy. PP2 (Src inhibitor), and Akt 1/2 kinase inhibitor were obtained from Sigma-Aldrich (St. Louis, MO). Antibodies used in this study were phospho-Src (Tyr419), total-Src, phospho-Akt (ser473), total-Akt, phospho-P130cas (Tyr410), phospho-paxillin (Tyr118), total-paxillin, phospho-FAK (Tyr576/577), phospho-FAK (Tyr925), CDC2, α/β-tubulin, and PARP (Cell Signaling Technology, Danvers, MA); total-P130cas (Thermo Scientific, Rockford, IL); total-FAK (BD Biosciences, San Jose, CA); phospho-FAK (pY397), phospho-FAK (pY861; Invitrogen, Camarillo, CA); glu-Tubulin, lamin B1 (Abcam, Cambridge, UK); CD31 (BD Pharmingen, San Diego, CA); Ki67 (Neomarkers Inc., Frement, CA); cleaved caspase-3 (Biocare Medical LLC, Concord, CA); β-actin (Sigma-Aldrich, St. Louis, MO); horseradish peroxidase–conjugated rat anti-mouse IgG2a (Serotec Harlan Bioproducts for Science Inc., Madison, WI); horseradish peroxidase–conjugated goat anti-rat IgG, and Alexa Fluor 488–conjugated anti-rabbit antibody (Jackson ImmunoResearch Laboratories, West Grove, PA).

In vivo orthotopic model of mucinous ovarian carcinoma

Female athymic nude mice were purchased from the National Cancer Institute-Frederick Cancer Research and Development Center (Frederick, MD), housed in specific pathogen-free conditions, and cared for in accordance with the guide lines set forth by the American Association for Accreditation for Laboratory Animal Care and the US Public Health Service Policy on Human Care and Use of Laboratory Animals. All animal experiments were approved and supervised by the MD Anderson Institutional Animal Care and Use Committee.

The *in vivo* model of mucinous ovarian carcinoma (RMUG-S-ip2 and RMUG-L-ip2) used in the present study has been described previously (15). RMUG-S-ip2 or RMUG-L-ip2 cells were inoculated into the peritoneal cavity of 40 orthotopic nude mice (4×10^6 cells per mouse). Mice were randomized into 4 treatment groups of 10 mice each: control, oxaliplatin, KX-01, and oxaliplatin plus KX-01. Treatments were initiated 4 weeks after inoculation. Oxaliplatin was dissolved in 5% dextrose and diluted with Hank's Balanced Salt Solution (HBSS) and administered intraperitoneally twice weekly (5 mg/kg per mouse) (22). KX-01 was solubilized in distilled water and administered orally every day (15 mg/kg per mouse, according to the dose finding experiment; see Figure S1A). Control mice received HBSS intraperitoneally twice weekly and oral distilled water daily. Mice were monitored on a daily basis and weighed weekly. After 8 weeks of treatment, the mice were sacrificed and total mouse body weight, tumor location and weight, and number of tumor nodules were recorded. Tumor specimens were preserved in either optimum cutting temperature medium (OCT; Miles Inc., Elkhart, IN; for frozen slides) or fixed in formalin (for paraffin slides) for further analysis.

Reverse phase protein arrays (RPPA)

RMUG-S and RMUG-L cells were treated with KX-01 at a concentration of 100 nM for 24 hours. Cells were homogenized using a digital homogenizer in the following lysis buffer: 1% Triton X-100, 50nM HEPES (pH 7.4), 150mM $MgCl_2$1mM EGTA, 100mM NaF, 10mM Na-pyrophosphate, 1mM $Na_3VO_4$10% glycerol, and freshly added protease and phosphatase inhibitors. Cellular proteins were denatured using 1% sodium dodecyl sulfate (SDS), and five 2× serial dilutions were performed in lysis buffer containing 1% SDS (dilution buffer). These diluted lysates were arrayed on nitrocellulose-coated FAST slides (Whatman Inc., Piscataway, NJ) using an Aushon 2470 Arrayer (Aushon BioSystems, Billerica, MA). Slides were probed with 152 validated primary antibodies and a biotin-conjugated secondary antibody. The Dako Cytomation-catalyzed system (Dako, Carpinteria, CA) was used for signal amplification. DAB colorimetric reaction was used for visualization. Slides were then scanned, analyzed, and quantified using customized Microvigene software (VigeneTech., North Billerica, MA), and spot intensity was generated.

A logistic model ("Supercurve Fitting," developed by the Department of Bioinformatics and Computational Biology at the MD Anderson Cancer Center; http://bioinformatics.mdanderson.org/OOMPA) was used to generate a fitted curve for each dilution. For both observed and fitted data, the fitted curve was then plotted with the signal intensities on the y-axis and the $\log_2$ concentration of proteins on the x-axis. From each slide, the protein concentrations were normalized using median polish. Positive fold-change was calculated by dividing each linear value (>1.0) by the average control linear value for each antibody tested, and negative fold-change (for linear values <1.0) was calculated using the formula (−1/linear fold-change) and plotted in a bar graph.

Western blot analysis

Cell lysates were obtained with RIPA lysis buffer (50mMTris-HCl [pH 7.4], 150mM NaCl, 1% Triton, 0.5% deoxycholate, 25 μg/mL leupeptin, 10 μg/mL aprotinin, 2mM EDTA, and 1mM sodium orthovanadate) and centrifuged for 15 minutes at 4°C. Protein concentration was then determined using the Bio-Rad Protein Assay Kit (Bio-Rad, Hercules, CA). Following protein loading (25μg/well), bands were separated on 8% gel using SDS-PAGE and transferred to nitrocellulose paper, blocked with 5% milk for 1 hour at room temperature, and incubated with primary antibodies overnight at 4°C. The bands were then incubated with horseradish peroxidase-conjugated anti-mouse or anti-rabbit (GE Healthcare, WI) for 1 hour at room temperature. Blots were developed using an enhanced chemiluminescence detection kit (Pierce Biotechnology, Rockford, IL). β-actin or vinculin was used for loading control, and all experiments were repeated in duplicate. Densitometry (Image J; National Institutes of Health) was used to assess the differences in results.

Cytotoxicity assays

Cells were plated in each well of a 96-well plate and maintained overnight. Cells were then exposed to KX-01 at concentrations of 1nM, 10nM, 100nM, 1000nM, or 10000nM for 48 or 72 hours, or to Akt1/2 inhibitor at concentrations of 1 μM, 5 μM, 10 μM, 50 μM, or 100 μM for 72 hours. Controls were treated with an equal volume of vehicle. To assess cell survival, 50 μL of 0.15% 3-(4,5-dimethylthiazol-2-yl)-2,5-diphenyltetrazolium bromide (MTT; Sigma-Aldrich) was added to each well and incubated for 2 hours at 37°C. The medium containing MTT was then removed and 100 μL of dimethyl sulfoxide (DMSO; Sigma-Aldrich) was added; cells were then incubated at room temperature for 10 minutes. Absorbance was then read at 570 nm by a 96-well Synergy HT-microplate reader (Ceres UV 900C; Bio-Tek Instrument Inc., Winooski, VT). Cell survival was defined as the percentage of cells surviving relative to the control group (number of viable cells in the treatment

group/number of viable cells in the control group). The experiments were repeated separately at least 3 times. The median inhibitory concentrations (IC50) were calculated.

Isobologram analysis was performed to evaluate the cytotoxicity of KX-01 and oxaliplatin in RMUG-S cells using dose-response cell-survival curves (23). The interaction index was calculated as described previously (24). Additive effects (equal to 1), synergistic effects (less than 1), and antagonistic effects (greater than 1) of the combination of oxaliplatin plus KX-01 were determined by the interaction index. Results were evaluated using R (version 2.14.2).

Cell proliferation assays

To determine cell proliferation, we used the Click-iT EdU Flow Cytometry Assay Kit (Invitrogen) according to the manufacturer's protocol. Briefly, cells were incubated with EdU for 2 hours before being harvested, then fixed with Click-iT fixative for 15 minutes at room temperature. After washing was completed, cells were permeabilized with Click-iTsaponin-based permeabilization and wash reagent for 15 minutes, and Click-iT reaction cocktail was added for 30 minutes. Cells were then analyzed using a Beckman Coulter XL 4-color flow cytometer (FACS; Beckman-Coulter, Miami, FL).

Apoptosis and cell cycle assays

Apoptosis was evaluated using the Annexin V-phycoerythrin (PE) apoptosis detection kit (BD Biosciences). Cells were incubated in trypsin-EDTA, and cell pellets were suspended in 1mL of 1× Annexin V binding buffer. One hundred microliters of each cell suspension was incubated with 5 μL of Annexin V-PE and 5 μL of 7-aminoactinomycin D (7–AAD) at room temperature (25°C) in the dark for 30 minutes. Following this incubation, 400 μL of 1× binding buffer was added to each tube, and samples were analyzed using FACS. Each experiment was repeated in triplicate.

For cell cycle analysis, cells were maintained in serum-free media for 24 hours and then lifted with trypsin, washed with phosphate-buffered saline (PBS), fixed in 70% cold ethanol, and stored overnight at 4°C. Cells were then centrifuged (pelleted) at 1,200 rotations per minute for 10 minutes at 4°C. After 1 wash with PBS, cells were suspended in propidium iodide (Roche, Indianapolis, IN) at 50 μg/mL and RNAseA (Qiagen, Valencia, CA) at 100 μg/mL and incubated in the dark at room temperature. Cells were then assessed for cell cycle status using FACS.

Immunohistochemical and immunofluorescence staining

Immunohistochemical staining was used to detect angiogenesis (CD31), cell proliferation (Ki67), and apoptosis (cleaved caspase-3) in frozen and paraffin-embedded tumor specimens. Paraffin sections were deparaffinized and rehydrated, then antigen retrieval was performed using citrate buffer (pH 6.0). Sections were then blocked with 3% hydrogen peroxide in methanol and 4% fish gelatin at room temperature, then incubated with Ki67 antibody (1:400) overnight at 4°C. After washing with PBS, the sections were incubated with horseradish peroxidase–conjugated rat anti-mouse IgG2a (1:100) for 1 hour. For cleaved caspase-3 staining, sections were treated similarly but incubated with the monoclonal mouse antibody against cleaved caspase-3 (1:100). For CD31 staining, frozen sections were fixed in cold acetone for 15 minutes, washed with PBS, endogenous proteins blocked (4% fish gelatin), and then incubated with rat monoclonal anti-mouse CD31 (1:800) overnight at 4°C. Sections were washed with PBS and incubated with horseradish peroxidase–conjugated goat anti-rat IgG (1:200) for 1 hour. Reactive tissues were visualized by staining with 3, 3-diaminobenzidine (Research Genetics, Huntsville, AL) and counterstaining with Gill's hematoxylin (BioGenex Laboratories, San Ramon, CA).

For quantification, 5 sections from each group were examined. To quantify microvessel density for each sample, the microvessels within 5 randomly selected 0.159-mm^2 fields at 200× magnification were counted. A single microvessel was defined as a discrete cluster or single cell stained positive for CD31 (CD31+). To quantify Ki67 and cleaved caspase-3, the percentage of positive cells was determined in 5 random 0.159-mm^2 fields at 200× magnification.

Tubulin and lamin B1 were analyzed by indirect immunofluorescence staining. Briefly, sections were fixed in cold acetone for 10 minutes, endogenous proteins blocked for 20 minutes at room temperature, incubated with tubulin antibody (α/β-tubulin; 1:50, glu-tubulin: 1:500) or lamin B1 antibody (1:1000) overnight at 4°C, and then incubated with Alexa Fluor 488–conjugated anti-rabbit antibody (1:1000) for 1 hour at room temperature. After washing with PBS, the samples were incubated with the DNA stain Hoechst 33342 (1:10000; Invitrogen) or DAPI (1:10000; Roche) for 10 minutes at room temperature. Mounted samples were visualized using a fluorescent microscope with the appropriate filter.

PTEN transfection and Src knockdown

For *PTEN* knock-in experiments, *PTEN* wild type cDNA was subcloned into the Not I site of a PLNCX expression vector (Clontech Laboratories, Mountain View, CA). *PTEN* mutants (G129R and PTZB) were generated using a standard mutagenesis method. For retrovirus production, 239T cells were transfected with vector using the calcium phosphate transfection method. Twenty-four hours after transfection, the standard media was replaced with media containing G418 sulfate (Mediatech Inc., Manassas, VA). After 1–2 weeks, cell lines stably infected with viral particles were established. The cells were treated with various concentrations of KX-01 for 72hours, and cell survival was assessed using the MTT assay. Src siRNA (Sence: CUGAGAGGGCGGUGGGUAUdTdT; Antisence: UACCCACCGCCCUCUCAGdTdT) was from Sigma-Aldrich. Transient knockdown experiments with siRNA were performed as described previously (25).

Statistical analysis

Continuous variables were assessed for normal distribution (Kolmogorov-Smirnov test) and expressed as appropriate (mean with standard deviation or median with range). Normally distributed variables were compared using the Student *t* test (2 groups) or analysis of variance (multiple groups). For variables with nonparametric distribution, the Mann-Whitney U test or Kruskal-Wallis test (multiple groups) was used. A p value <0.05 in 2-tailed testing was deemed statistically significant. The Statistical Package for Social Scientists software (SPSS, version 18.0; SPSS, Inc., Chicago, IL) was used for all analyses.

For the RPPA data analysis, to limit the false discovery rate to 5%, each cell line was examined individually. We first completed a 2 × 2 factorial analysis of variance to detect a treatment effect on expression and then used the beta-uniform mixture distribution method (26) to determine a p value cutoff for statistical significance that would limit our false discovery rate to 5%. Finally, if a treatment effect was evident, we tested for differences between KX-01 and control. After examining each cell line, we used t-tests to determine whether RMUG-S controls differed from RMUG-L controls. We then employed the beta-uniform mixture method again to limit our false discovery rate to 5%. Linear fold-change was calculated by dividing each linear value by the average control linear value. Positive fold-change (>1.0) was the same as the linear fold-change value; negative fold-change (for linear values <1.0) was calculated as −1/linear fold-change.

RESULTS

In vivo effects of KX-01 in tumor xenografts

To recapitulate the unique features of mucinous ovarian carcinoma, we have recently established an orthotopic mouse model of metastatic mucinous ovarian carcinoma (15). The RMUG-S and RMUG-L models were utilized to evaluate the biological effects of KX-01 *in vivo*. In the RMUG-S model, tumor weight was reduced by 75% ($p<0.001$) and tumor nodules decreased ($p<0.01$) following treatment with KX-01 compared with the control group (Figure 1A). In the RMUG-L model, tumor weight was reduced by 50% and 48% fewer tumor nodules were observed in the KX-01 treatment group compared with the control group ($p<0.05$; Figure 1B).

Because oxaliplatin shows potential as a chemotherapeutic drug for mucinous ovarian carcinoma, we also evaluated the effects KX-01 in combination with oxaliplatin in the RMUG-S and RMUG-L models. In the RMUG-S model, tumor weight was reduced by 90% ($p<0.0001$) and 85% fewer tumor nodules ($p<0.001$) were observed in the combination group compared with the control group (Figure 1A). Combination therapy led to significantly greater tumor suppression effects than did either monotherapy (combination vs. KX-01, oxaliplatin, 90% vs. 75%, 72%, $p<0.05$). In the RMUG-L model, while a significant reduction in tumor weight and number of nodules was observed in the combination group compared with the control group, the antitumor effects of the combination therapy did not differ from those of either monotherapy ($p>0.05$; Figure 1B), signifying that the antitumor effects of the combination therapy were greater in the RMUG-S model than in the RMUG-L model. The body weight of the mice after treatment did not differ between the treatment and control groups in either the RMUG-S or RMUG-L model (Figure S1B, S1C).

To investigate potential mechanisms of KX-01's antitumor activity, we tested markers of cell proliferation (Ki67), angiogenesis (CD31), and apoptosis (cleaved caspase-3) in the tumor tissues. In the RMUG-S model, tumor cell proliferation was reduced in both the KX-01 group (33% reduction, $p<0.05$) and the oxaliplatin group (29% reduction, $p<0.05$) compared with the control group. Tumor cell proliferation was most significantly decreased in the combination group compared with the control group (47% reduction, $p<0.01$; Figure 1C). Tumor angiogenesis was significantly reduced in all KX-01-based treatment groups compared with the control group (KX-01 vs. control, 43% reduction, $p<0.01$; combination vs. control, 69% reduction, $p<0.0001$; Figure 1D). This difference was not observed in the oxaliplatin group compared with the control group ($p>0.05$; Figure 1D).

Tumor cell apoptosis was increased in the oxaliplatin and KX-01 groups compared with the control group ($p<0.05$; Figure 1E), with the greatest increase in the combination group ($p<0.01$; Figure 1E). In the RMUG-L model, similar biological effects of KX-01 on angiogenesis and cell apoptosis were observed, but the effects of KX-01 on cell proliferation were less pronounced than in the RMUG-S model (21% reduction in RMUG-L vs. 33% reduction in RMUG-S, $p<0.01$; Figure S2).

In vitro effects of KX-01 in mucinous ovarian carcinoma cells

To identify potential mechanisms by which KX-01 exerts its antitumor activity, we next tested its effects on cell survival, proliferation, apoptosis and migration in mucinous ovarian cancer cells. Treatment with KX-01 consistently resulted in decreased cell survival in RMUG-S, RMUG-L, YDOV-151, and EFO-27 mucinous ovarian carcinoma cells with IC50 levels from 72nM – 203nM (Figure 2A). Similar effects on survival were also noted in clear cell ovarian cancer cell lines (Figure S3A). In the RMUG-L cells, the inhibition rate did not reach 50%, indicating the relative resistance of RMUG-L cells to KX-01 treatment. KX-01

treatment reduced proliferation by 73% (*vs.* control, p<0.001) in RMUG-S cells, and 46% (*vs.* control, p< 0.01) in RMUG-L cells (Figure 2B). KX-01 induced comparable late apoptosis in both cell lines (Figure 2C). Immunoblotting demonstrated that cleaved PARP expression was significantly increased after KX-01 treatment in both cell lines (Figure S3B). A shift toward the G2/M phase was seen in cells treated with KX-01 (Figure 2D). Further, KX-01 inhibited the migration of both cell lines (Figure S3C, S3D).

We also tested the effects of various concentrations of combined oxaliplatin and KX-01 in RMUG-S cells. The IC50 of oxaliplatin alone was 14μg/mL; the effects of oxaliplatin, based on increased apoptosis, were significantly enhanced with KX-01 (Figure 2E, 2F). In isobologram analysis, the interaction index was <1 at all examined points, suggesting synergistic effects of oxaliplatin and KX-01 (Figure 2G).

Since KX-01 has activity against Src and tubulin, we investigated the effects of a pure Src inhibitor (PP2) or paclitaxel in RMUG-S cells. PP2 had minimal effects on cell survival (Figure S4A), and paclitaxel had effects on cell survival at higher concentrations (IC50=147 ng/mL; Figure S4B). The greater effect observed with KX-01 (Figure 2A) may be secondary to dual targeting of Src and tubulin. The effects of Src siRNA, PP2 or paclitaxel with oxaliplatin were also tested, demonstrating that Src siRNA and PP2, but not paclitaxel, resulted in lower IC50 level of oxaliplatin (Figure S4C, S4D, S4E).

Pathways affected by KX-01 treatment in mucinous ovarian carcinoma cells

Because KX-01 was constructed to inhibit phosphorylation of Src substrates, we also tested the effects of KX-01 on Src and FAK, and various Src substrates (Akt, paxillin, and P130cas). In the sensitive RMUG-S cells, expression of p-Akt (ser473), p-paxillin (Tyr118), and p-P130cas (Tyr410) was significantly lower in cells treated with various concentrations of KX-01 for 24 hours than in control cells (Figure 3A). In RMUG-L cells, expression of p-paxillin (Tyr118) and p-P130cas (Tyr410) was significantly lower while expression of p-Akt (ser473) was higher in cells treated with KX-01 than in control cells (Figure 3B). Expression of p-Src (Tyr416), total-Src, p-FAK (pY397, Tyr576/577, pY861, Tyr925), and total-FAK was not significantly different between the treatment and control cells (data not shown).

The effects of treatment with oxaliplatin alone and the combination of oxaliplatin plus KX-01 on the expression and activation of Src substrates were analyzed in the RMUG-S cell line. Induction of P-Akt, p-paxillin, and p-P130cas activity was seen in the cells in response to oxaliplatin monotherapy, whereas KX-01 blocked oxaliplatin induced p-Akt, p-paxillin, and p-P130cas levels in the cells treated with the combination therapy (Figure 3C).

To explore other potential pathways disturbed by KX-01, we utilized RPPAs. This analysis demonstrated that KX-01 inhibited p-Akt (Ser473) expression in RMUG-S cells, but not in RMUG-L cell, consistent with our Western blot results (Table S1, S2; Figure S5A, S5B). Expression of 72 molecules in RMUG-S cells and 60 molecules in RMUG-L cells significantly differed between cells treated with KX-01 and control cells, and expression of 35 of these molecules differed between treatment and control cells in both RMUG-S and RMUG-L cells (p<0.05; Figure 3D, S5A, S5B). The majority of these proteins were direct or indirect downstream SFK members, acute stress-inducing proteins (MAPK pathway), and those associated with apoptosis and cell cycle regulation (Figure 3E).

In both RMUG-S and RMUG-L cells treated with KX-01, expression of most SFK downstream proteins, such as p-p70s6k, p-S6, and mTOR, were inhibited, and expression of acute stress-inducing and apoptosis-related proteins was increased. However, changes in expression of proteins associated with cell cycle regulation were completely opposite in the 2 cell lines, except for p21 (Figure 3E); cyclin B1/CDC2 protein expression with Western

blot confirmed these results (Figure S5C). Since one of the functions of cyclin B1 in combination with CDC2 (CDK1) is nuclear membrane breakdown, we stained RMUG-S and L cells with lamin B1 after treatment with KX-01. Lamin B1 in the nuclear membrane was disrupted to a greater extent in the RMUG-S cells than RMUG-L cells (Figure S5D, S5E). This suggests the relative sensitivity of RMUG-S and resistance of RMUG-L cells to KX-01 observed may be related to cell cycle proteins.

KX-01 inhibited tubule polymerization and disrupted the microtubule network

To test whether KX-01 could directly affect the organization of the microtubule network, we treated RMUG-S and RMUG-L cells with KX-01 or vehicle for 24 or 48 hours and subsequently fixed and stained the cells with FITC-conjugated anti-α/β-tubulin antibody and Hoechst 33342 or DAPI for *in situ* observation of the microtubule network and nuclei with fluorescence microscopy. The microtubule network in control cells exhibited normal arrangement, with microtubules traversing intricately throughout the cell, and nuclei were intact and normal in appearance (Figure 4A, 4B, S6A, S6B). In contrast, cells treated with KX-01 had a smaller microtubule network, with a diffuse stain visible throughout the cytoplasm. Compared with RMUG-L cells, microtubules in RMUG-S cells were affected to a greater extent after treatment with KX-01 (Figure 4A, 4B, S6A, S6B). Condensation and fragmentation of nuclei were apparent in cells treated with KX-01 (Figure 4A, 4B). Moreover, endoreduplication was also observed in cells treated with KX-01 (Figure 4B, S6A).

In tumor tissue from orthotopic mouse models, the staining patterns were similar to those of the *in vitro* tumor cells, and fluorescence intensity was markedly reduced in the KX-01 and combination groups compared with the control group (Figure 4C, 4D). In the oxaliplatin group, the staining pattern of tubulin was unchanged from the control group (Figure 4C, 4D).

PTEN status affects mucinous ovarian carcinoma cell sensitivity to KX-01

As shown, p-Akt (Ser473) was reduced by KX-01 in the sensitive RMUG-S cells, but not in RMUG-L cells. Expression of p-Akt (Ser473) was significantly higher in RMUG-L cells compared to RMUG-S cells (Figure 3A, 3B). Given that *PTEN* regulates Akt activity *via* inhibition of Akt phosphorylation, we examined *PTEN* status in both cell lines to explore potential underlying mechanisms involved in sensitivity to KX-01. *PTEN* is wild-type in RMUG-S cells, while RMUG-L cells have absent *PTEN* expression (Figure S7A). As previous studies have shown that *PTEN* deficiency is associated with *de novo* resistance to epidermal growth factor receptor inhibitors (27–28), we examined the relationship between *PTEN* deficiency and response to KX-01 in RMUG-L cells. RMUG-L cells were transfected with wild type or domain mutant (G129R, PTZB) *PTEN* and then exposed to various concentrations of KX-01 for 72 hours. Sensitivity to KX-01 was significantly enhanced in *PTEN*-restored cells; IC50 was undetectable in the control cells, but was 464 nM in the *PTEN*-restored cells. In RMUG-L cells transfected with mutant *PTEN*the sensitivity to KX-01 did not differ from that of control cells (Figure 5A). Next, we assessed cell proliferation, apoptosis, and cell cycle status in control, wild type, and *PTEN* domain mutant RMUG-L cells treated with KX-01. In *PTEN* wild-type cells, compared with control and domain mutant cells, cell proliferation was significantly inhibited, apoptosis was significantly increased, and the proportion of S phase cells was significantly decreased (Figure 5B, 5C, 5D). In addition, Western blot showed that expression of p-Akt (ser473) and CDC2 was significantly inhibited in *PTEN* wild-type cells, whereas no change in expression was observed in the control and *PTEN* domain mutant cells (Figure 5E).

Because *PTEN* is associated with lower levels of p-Akt (29), we also tested both RMUG-S and RMUG-L cells for sensitivity to an Akt1/2 inhibitor. Both RMUG-S and RMUG-L cells were sensitive to the Akt1/2 inhibitor (Figure S7BD), and p-Akt expression was significantly decreased in both RMUG-S and RMUG-L cells after treatment with the Akt1/2 inhibitor (Figure S7C).

DISCUSSION

This study establishes the ability of KX-01 to suppress cell growth effectively through targeting of both the Src pathway and tubulin in mucinous ovarian carcinoma cells *in vitro* and *in vivo*and highlights *PTEN* deletion as a predictor of poor response to KX-01 treatment. Further, KX-01 demonstrates synergistic antitumor activity in combination with oxaliplatin. These data suggest targeting both the Src pathway and tubulin with KX-01alone, or in combination with oxaliplatin, may represent a more promising treatment for mucinous ovarian carcinoma than those currently available.

Preclinical studies in estrogen receptor-positive and estrogen receptor/progesterone receptor/HER2-negative breast cancers have demonstrated that KX-01 reduced proliferation and angiogenesis and increased apoptosis in xenograft tumors, and led to synergistic growth inhibition when combined with chemotherapeutic drugs (30–31). KX-01 is currently in phase I/II clinical trials for the treatment of malignancies, including prostate cancer and acute myeloid leukemia (30).

Our RPPA data demonstrate that KX-01 significantly increased expression of MAPK pathway proteins, including p38, p-JNK, and p-Jun. Because microtubule disruption has been shown to activate MAPK pathway molecules (32), alterations of p38, p-JNK, and p-Jun observed after treatment with KX-01 suggest that it leads to microtubule disruption. Immunofluorescence staining confirms that the microtubule network in both cells lines was disrupted by KX-01, and the appearance of the microtubules after treatment with KX-01 was similar to the appearance of microtubules after treatment with another tubulin polymerization inhibitory reagent (33). RPPA data did not demonstrate alterations in tubulin levels in RMUG-S and RMUG-L cells, suggesting that KX-01 may disrupt microtubule structure and organization, but not affect tubulin expression levels. As seen with other microtubule inhibitors, endoreduplication was observed in cells following treatment with KX-01(34).

Our *PTEN* knock-in experiments reveal that *PTEN* mutation may contribute to relative resistance to KX-01. Cell proliferation and cell cycle data showed that the inhibition of cell proliferation and the proportion of S phase cells differed between RMUG-S and RMUG-L cells, suggesting proteins that regulate cell proliferation and cell cycle may be involved in the resistance of mucinous ovarian carcinoma cells to KX-01. Changes in expression of cell cycle–regulating molecules such as CDK1 (CDC2) and cyclin B1 differed between RMUG-S and RMUG-L cells. CDK1 is a core component of the cell cycle machinery, combining with cyclin B1 (CDK1/cyclin B1) to promote S, G2, and M phase progression (35–36). Recently published data also showed that CDK1 activity promoted cell proliferation and survival and was associated with resistance to therapy (37), and inhibition of CDK1 was shown to induce cell death and block tumor growth (38), leading us to suspect that CDK1 may be involved in decreased response to KX-01. In our *PTEN*-restored RMUG-L cells, KX-01 inhibited the cell proliferation and the proportion of S phase cells to a greater extent than in control cells or *PTEN* domain mutant cells without significant effects on the proportion of G1 and G2/M phases. Since S phase involves DNA replication, and CDK1 activity is essential for DNA replication (39), it is possible that the inhibition of S phase in PTEN-restored cells may be due to inhibition of CDK1 by KX-01. Because the PI3K/Akt

pathway contributes to cyclin B1 expression and CDK1 activation (40), these results suggest that the PTEN-PI3K/Akt-CDK1 axis plays a role in response to KX-01.

Because mucinous ovarian carcinoma histologically and molecularly mimics colorectal carcinoma, oxaliplatin, a chemotherapeutic agent considered standard treatment for advanced-stage colorectal carcinoma, is a logical prospect in the treatment of mucinous ovarian carcinoma (15, 41). Sato et al. showed that 2 of the 5 mucinous ovarian carcinoma cell lines examined were sensitive to oxaliplatin, and the combination of oxaliplatin and fluorouracil was significantly inhibitory in 4 of the 5 cell lines (42). On the basis of these studies, we combined KX-01 with oxaliplatin in our experiments. Both our *in vitro* and *in vivo* experiments show the combination to be synergistic, resulting in enhanced antitumor activity compared with either monotherapy alone. These results validate the potential of the combination treatment strategy for translation to the clinical setting.

The mechanism underling the synergic effect of combination therapy is not completely clear. Our previous data showed that treatment with oxaliplatin alone induced Src kinase activity, which has been proposed as a potential mechanism of resistance to oxaliplatin in mucinous ovarian carcinoma, and that adding the Src/Abl inhibitor dasatinib to the treatment with oxaliplatin could attenuate the oxaliplatin-induced Src kinase activity, leading to synergistic effects (15). Because induction of Src kinase activity is thought to be associated with drug resistance via the Akt and Ras pathways (22, 43), our results suggest that KX-01 may inhibit oxaliplatin-induced expression of p-Akt, leading to the synergistic effects of the combination therapy.

In summary, our results demonstrate that KX-01 significantly suppresses mucinous ovarian carcinoma by targeting both Src substrates and tubulin. These dual effects may make KX-01 a particularly effective treatment for mucinous ovarian carcinoma. In addition, our results suggest that *PTEN* mutation may be a predictive biomarker of response to KX-01 treatment. Clinical studies employing KX-01 in the treatment of mucinous ovarian carcinoma and investigating *PTEN* mutation as a potential biomarker are warranted.

Supplementary Material

Refer to Web version on PubMed Central for supplementary material.

Acknowledgments

We thank Tamara Locke in the Department of Scientific Publications at M. D. Anderson Cancer Center for editing our manuscript. We also thank Kinex Pharmaceuticals for providing KX-01.

GRANT SUPPORT

Financial support was provided by the National Institutes of Health (P50 CA098258, CA109298, P50 CA083639, CA016672, CA128797, U54 CA151668), the CPRIT (RP110595), the Ovarian Cancer Research Fund, Inc. (Program Project Development Grant), the U.S. Department of Defense (OC073399, OC093146), the Taiwan National Science Council (NSC-96-3111-B), the Zarrow Foundation, the Marcus Foundation, the Betty Anne Asche Murray Distinguished Professorship, National Cancer Institute institutional Core Grant CA16672, and the Laura and John Arnold Foundation. BZ and HJD are supported by an NCI-DHHS-NIH T32 Training Grant (T32 CA101642).

REFERENCES

1. Hess V, A'Hern R, Nasiri N, King DM, Blake PR, Barton DP, et al. Mucinous epithelial ovarian cancer: a separate entity requiring specific treatment. J Clin Oncol. 2004; 22:1040–1044. [PubMed: 15020606]

2. Frumovitz M, Schmeler KM, Malpica A, Sood AK, Gershenson DM. Unmasking the complexities of mucinous ovarian carcinoma. Gynecol Oncol. 2010; 117:491–496. [PubMed: 20332054]
3. Pectasides D, Fountzilas G, Aravantinos G, Kalofonos HP, Efstathiou E, Salamalekis E, et al. Advanced stage mucinous epithelial ovarian cancer: the Hellenic Cooperative Oncology Group experience. Gynecol Oncol. 2005; 97:436–441. [PubMed: 15863142]
4. Pisano C, Greggi S, Tambaro R, Losito S, Iodice F, Di Maio M, et al. Activity of chemotherapy in mucinous epithelial ovarian cancer: a retrospective study. Anticancer Res. 2005; 25:3501–3505. [PubMed: 16101169]
5. Bamias A, Psaltopoulou T, Sotiropoulou M, Haidopoulos D, Lianos E, Bournakis E, et al. Mucinous but not clear cell histology is associated with inferior survival in patients with advanced stage ovarian carcinoma treated with platinum-paclitaxel chemotherapy. Cancer. 2010; 116:1462–1468. [PubMed: 20108307]
6. Shimada M, Kigawa J, Ohishi Y, Yasuda M, Suzuki M, Hiura M, et al. Clinicopathological characteristics of mucinous adenocarcinoma of the ovary. Gynecol Oncol. 2009; 113:331–334. [PubMed: 19275957]
7. Alexandre J, Ray-Coquard I, Selle F, Floquet A, Cottu P, Weber B, et al. Mucinous advanced epithelial ovarian carcinoma: clinical presentation and sensitivity to platinum-paclitaxel-based chemotherapy, the GINECO experience. Ann Oncol. 2010; 21:2377–2381. [PubMed: 20494964]
8. Naik JD, Seligmann J, Perren TJ. Mucinous tumours of the ovary. J Clin Pathol. 2012; 65:580–584. [PubMed: 22011449]
9. Kim LC, Song L, Haura EB. Src kinases as therapeutic targets for cancer. Nat Rev Clin Oncol. 2009; 6:587–595. [PubMed: 19787002]
10. Yeatman TJ. A renaissance for SRC. Nat Rev Cancer. 2004; 4:470–480. [PubMed: 15170449]
11. Kopetz S, Shah AN, Gallick GE. Src continues aging: current and future clinical directions. Clin Cancer Res. 2007; 13:7232–7236. [PubMed: 18094400]
12. Jallal H, Valentino ML, Chen G, Boschelli F, Ali S, Rabbani SA. A Src/Abl kinase inhibitor, SKI-606, blocks breast cancer invasion, growth, and metastasis in vitro and in vivo. Cancer Res. 2007; 67:1580–1588. [PubMed: 17308097]
13. Serrels A, Macpherson IR, Evans TR, Lee FY, Clark EA, Sansom OJ, et al. Identification of potential biomarkers for measuring inhibition of Src kinase activity in colon cancer cells following treatment with dasatinib. Mol Cancer Ther. 2006; 5:3014–3022. [PubMed: 17148760]
14. Nam S, Kim D, Cheng JQ, Zhang S, Lee JH, Buettner R, et al. Action of the Src family kinase inhibitor, dasatinib (BMS-354825), on human prostate cancer cells. Cancer Res. 2005; 65:9185–9189. [PubMed: 16230377]
15. Matsuo K, Nishimura M, Bottsford-Miller JN, Huang J, Komurov K, Armaiz-Pena GN, et al. Targeting SRC in mucinous ovarian carcinoma. Clin Cancer Res. 2011; 17:5367–5378. [PubMed: 21737505]
16. Puls LN, Eadens M, Messersmith W. Current status of SRC inhibitors in solid tumor malignancies. Oncologist. 2011; 16:566–578. [PubMed: 21521831]
17. Adjei AA, Cohen RB, Kurzrock R, Gordon GS, Hangauer D, Dyster L, et al. Results of a phase I trial of KX2-391, a novel non-ATP competitive substrate-pocket directed SRC inhibitor, in patients with advanced malignancies. Journal of Clinical Oncology. 2009; 27
18. Hangauer DG, Smolinski M, Bu YH, Kazim L, Qu J. Photoaffinity labeling studies to better define the mechanism of action for Phase II oncology drug KX2-391. Abstr Pap Am Chem S. 2010; 239
19. Kunzmann R, Holzel F. Karyotype alterations in human ovarian carcinoma cells during long-term cultivation and nude mouse passage. Cancer Genet Cytogenet. 1987; 28:201–212. [PubMed: 3476184]
20. Cho H, Lim BJ, Kang ES, Choi JS, Kim JH. Molecular characterization of a new ovarian cancer cell line, YDOV-151, established from mucinous cystadenocarcinoma. Tohoku J Exp Med. 2009; 218:129–139. [PubMed: 19478469]
21. Lee JW, Stone RL, Lee SJ, Nam EJ, Roh JW, Nick AM, et al. EphA2 targeted chemotherapy using an antibody drug conjugate in endometrial carcinoma. Clin Cancer Res. 2010; 16:2562–2570. [PubMed: 20388851]

22. Kopetz S, Lesslie DP, Dallas NA, Park SI, Johnson M, Parikh NU, et al. Synergistic activity of the SRC family kinase inhibitor dasatinib and oxaliplatin in colon carcinoma cells is mediated by oxidative stress. Cancer Res. 2009; 69:3842–3849. [PubMed: 19383922]
23. Machado SG, Robinson GA. A direct, general approach based on isobolograms for assessing the joint action of drugs in pre-clinical experiments. Stat Med. 1994; 13:2289–2309. [PubMed: 7855464]
24. Chou TC. Drug combination studies and their synergy quantification using the Chou-Talalay method. Cancer Res. 2010; 70:440–446. [PubMed: 20068163]
25. Nick AM, Stone RL, Armaiz-Pena G, Ozpolat B, Tekedereli I, Graybill WS, et al. Silencing of p130cas in ovarian carcinoma: a novel mechanism for tumor cell death. J Natl Cancer Inst. 2011; 103:1596–1612. [PubMed: 21957230]
26. Pounds S, Cheng C. Improving false discovery rate estimation. Bioinformatics. 2004; 20:1737–1745. [PubMed: 14988112]
27. Sos ML, Koker M, Weir BA, Heynck S, Rabinovsky R, Zander T, et al. PTEN loss contributes to erlotinib resistance in EGFR-mutant lung cancer by activation of Akt and EGFR. Cancer Res. 2009; 69:3256–3261. [PubMed: 19351834]
28. Nagata Y, Lan KH, Zhou X, Tan M, Esteva FJ, Sahin AA, et al. PTEN activation contributes to tumor inhibition by trastuzumab, and loss of PTEN predicts trastuzumab resistance in patients. Cancer Cell. 2004; 6:117–127. [PubMed: 15324695]
29. Yin Y, Shen WH. PTEN: a new guardian of the genome. Oncogene. 2008; 27:5443–5453. [PubMed: 18794879]
30. Anbalagan M, Ali A, Jones RK, Marsden CG, Sheng M, Carrier L, et al. Peptidomimetic Src/Pretubulin Inhibitor KX-01 Alone and in Combination with Paclitaxel Suppresses Growth, Metastasis in Human ER/PR/HER2-Negative Tumor Xenografts. Mol Cancer Ther. 2012; 11:1936–1947. [PubMed: 22784709]
31. Anbalagan M, Carrier L, Glodowski S, Hangauer D, Shan B, Rowan BG. KX-01, a novel Src kinase inhibitor directed toward the peptide substrate site, synergizes with tamoxifen in estrogen receptor alpha positive breast cancer. Breast Cancer Res Treat. 2012; 132:391–409. [PubMed: 21509526]
32. Stone AA, Chambers TC. Microtubule inhibitors elicit differential effects on MAP kinase (JNK, ERK, p38) signaling pathways in human KB-3 carcinoma cells. Exp Cell Res. 2000; 254:110–119. [PubMed: 10623471]
33. Zhang LH, Wu L, Raymon HK, Chen RS, Corral L, Shirley MA, et al. The synthetic compound CC-5079 is a potent inhibitor of tubulin polymerization and tumor necrosis factor-alpha production with antitumor activity. Cancer Res. 2006; 66:951–959. [PubMed: 16424030]
34. Stewart ZA, Mays D, Pietenpol JA. Defective G1-S cell cycle checkpoint function sensitizes cells to microtubule inhibitor-induced apoptosis. Cancer Res. 1999; 59:3831–3837. [PubMed: 10447002]
35. Hochegger H, Dejsuphong D, Sonoda E, Saberi A, Rajendra E, Kirk J, et al. An essential role for Cdk1 in S phase control is revealed via chemical genetics in vertebrate cells. J Cell Biol. 2007; 178:257–268. [PubMed: 17635936]
36. Malumbres M, Barbacid M. Cell cycle, CDKs and cancer: a changing paradigm. Nat Rev Cancer. 2009; 9:153–166. [PubMed: 19238148]
37. Liu P, Kao TP, Huang H. CDK1 promotes cell proliferation and survival via phosphorylation and inhibition of FOXO1 transcription factor. Oncogene. 2008; 27:4733–4744. [PubMed: 18408765]
38. Goga A, Yang D, Tward AD, Morgan DO, Bishop JM. Inhibition of CDK1 as a potential therapy for tumors over-expressing MYC. Nature Medicine. 2007; 13:820–827.
39. Hochegger H, Dejsuphong D, Sonoda E, Saberi A, Rajendra E, Kirk J, Hunt T, Takeda S. An essential role for Cdk1 in S phase control is revealed via chemical genetics in vertebrate cells. J Cell Biol. 2007; 178:257–268. [PubMed: 17635936]
40. Roberts EC, Shapiro PS, Nahreini TS, Pages G, Pouyssegur J, Ahn NG. Distinct cell cycle timing requirements for extracellular signal-regulated kinase and phosphoinositide 3-kinase signaling pathways in somatic cell mitosis. Mol Cell Biol. 2002; 22:7226–7241. [PubMed: 12242299]

41. Cunningham D, Atkin W, Lenz HJ, Lynch HT, Minsky B, Nordlinger B, et al. Colorectal cancer. Lancet. 2010; 375:1030–1047. [PubMed: 20304247]

42. Sato S, Itamochi H, Kigawa J, Oishi T, Shimada M, Naniwa J, et al. Combination chemotherapy of oxaliplatin and 5-fluorouracil may be an effective regimen for mucinous adenocarcinoma of the ovary: a potential treatment strategy. Cancer Sci. 2009; 100:546–551. [PubMed: 19154404]

43. Peterson-Roth E, Brdlik CM, Glazer PM. Src-Induced cisplatin resistance mediated by cell-to-cell communication. Cancer Res. 2009; 69:3619–3624. [PubMed: 19351863]

Translational Relevance

Mucinous ovarian carcinoma responds poorly to currently available treatments. Recently, we reported that Src kinase is overexpressed in mucinous ovarian carcinoma, and a Src inhibitor significantly inhibited tumor growth and enhanced the antitumor effects of oxaliplatin. In this study, we show that KX-01 (Src and tubulin inhibitor) significantly inhibits cell proliferation, induces apoptosis, arrests the cell cycle at the G2/M phase in mucinous ovarian cancer cell lines, and suppresses tumor growth in preclinical mucinous ovarian cancer models. Moreover, KX-01 showed synergistic antitumor activity when combined with oxaliplatin. These findings suggest that targeting both Src and tubulin may be a promising therapeutic approach for patients with mucinous ovarian carcinoma.

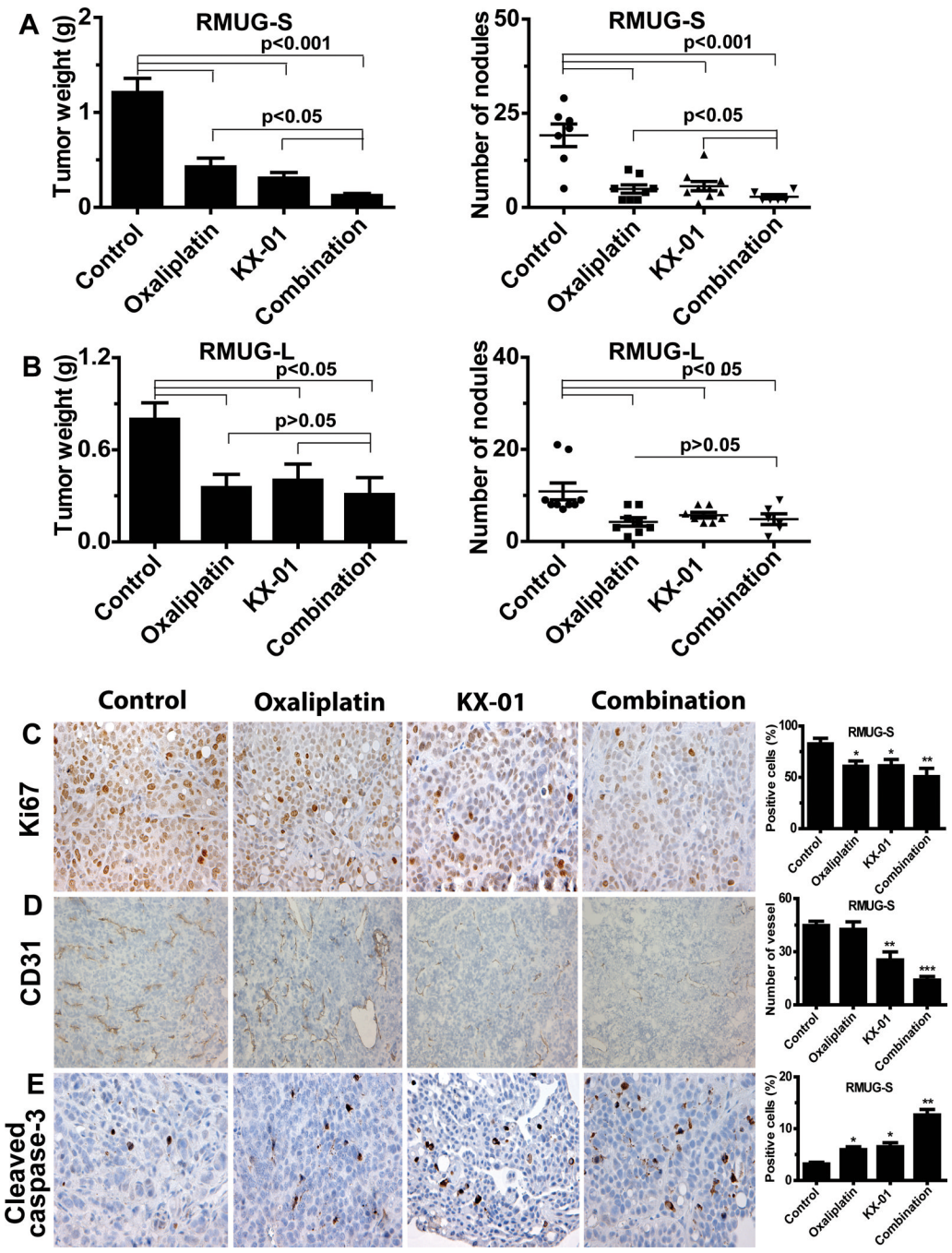

Figure 1.

(**A, B**) Anti-tumor activity of KX-01 and oxaliplatin in (**A**) RMUG-S and (**B**) RMUG-L mouse models of mucinous ovarian carcinoma. Mice were randomized to four groups (n=10 mice per group) and underwent treatment as follows: (1) control group, (2) oxaliplatin group, (3) KX-01 group, and (4) combination group. Data are shown as mean ± standard deviation (error bars). (**C, D, E**) Effects of KX-01 and oxaliplatin on cell proliferation (Ki-67; **C**), angiogenesis (CD31; **D**), and apoptosis (Cleaved caspase-3; **E**) in the RMUG-S mouse model. Original magnification 200×. Bars in the graphs correspond sequentially to

the labeled columns of images on the left. Data are shown as mean ± SEM (error bars). *p<0.05, **p<0.01, *** p<0.0001 compared with the control group.

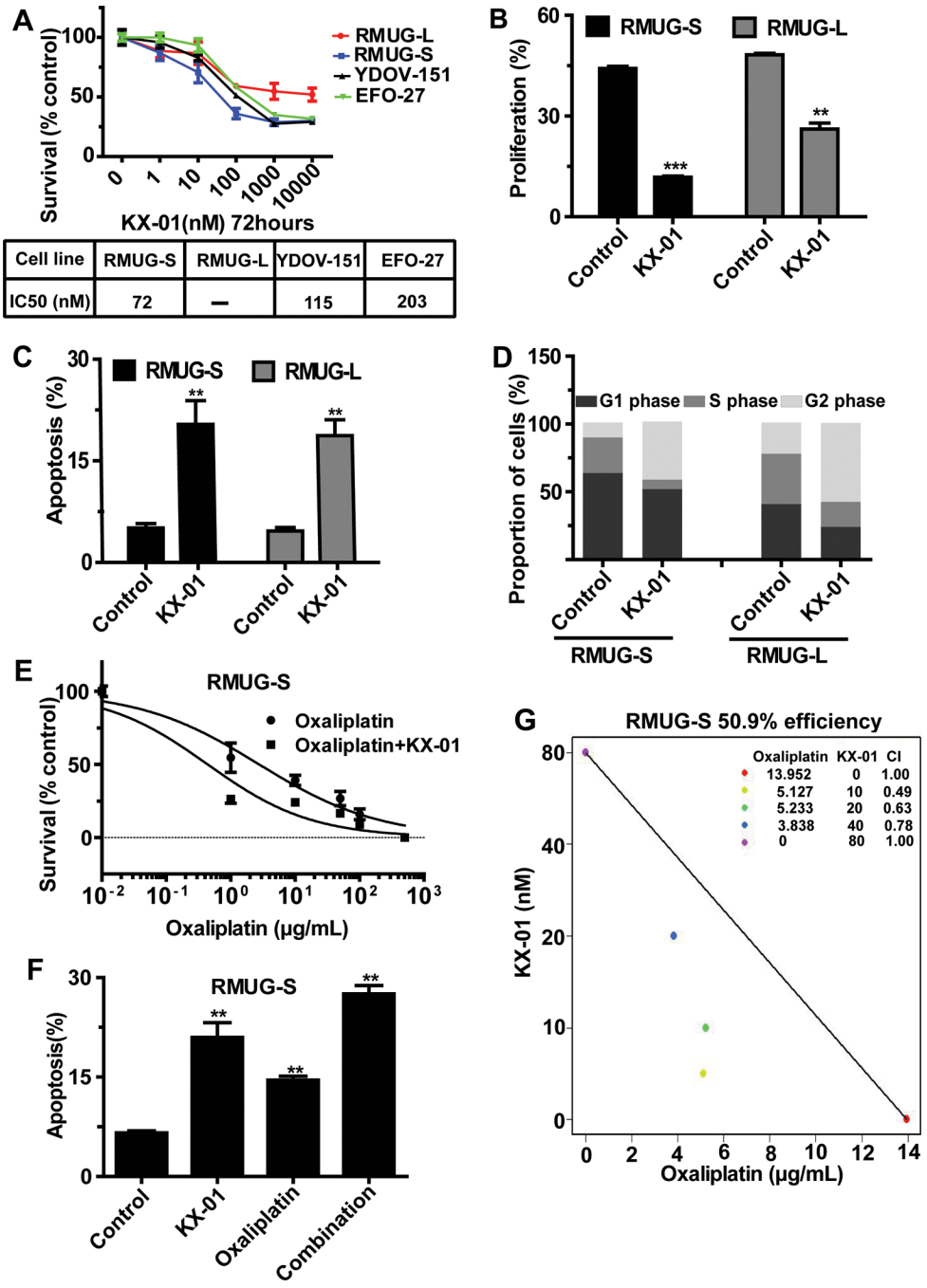

Figure 2.

Biological effects of KX-01 on mucinous ovarian carcinoma cells in vitro. (**A**) MTT assay results showing the effect of KX-01 on cell survival at various concentrations in a panel of mucinous ovarian carcinoma cells. Cell survival was calculated as the number of cells surviving relative to the number of cells surviving in the control group. IC50 indicates median inhibitory rate. (**B**) EdU assay results showing inhibition of cell proliferation in cells treated with KX-01 compared with control cells in RMUG-S and RMUG-L cells. (**C**) Annexin V and 7-aminoactinomycin D assay results showing cell apoptosis in cells treated with KX-01 compared with control cells in RMUG-S and RMUG-L cells. (**D**) Flow

cytometry results showing induction of mitotic arrest in cells treated with KX-01 compared with control cells in RMUG-S and RMUG-L cells. (**E**) Cell cytotoxicity in RMUG-S cells treated with various concentrations of oxaliplatin with or without 100nM KX-01 for 72 hours. Results are presented as in **A**. (**F**) Isobologram analysis for the combination of KX-01 and oxaliplatin in RMUG-S cells. The interaction index was <1 at all examined points. (**G**) Apoptosis in RMUG-S cells after treatment with 15 μg/mL oxaliplatin, 100nM KX-01, or a combination of both treatments for 72 hours. All experiments were repeated at least 3 times, and bars represent means with standard errors. **p<0.01, ***p<0.001 compared with the control group.

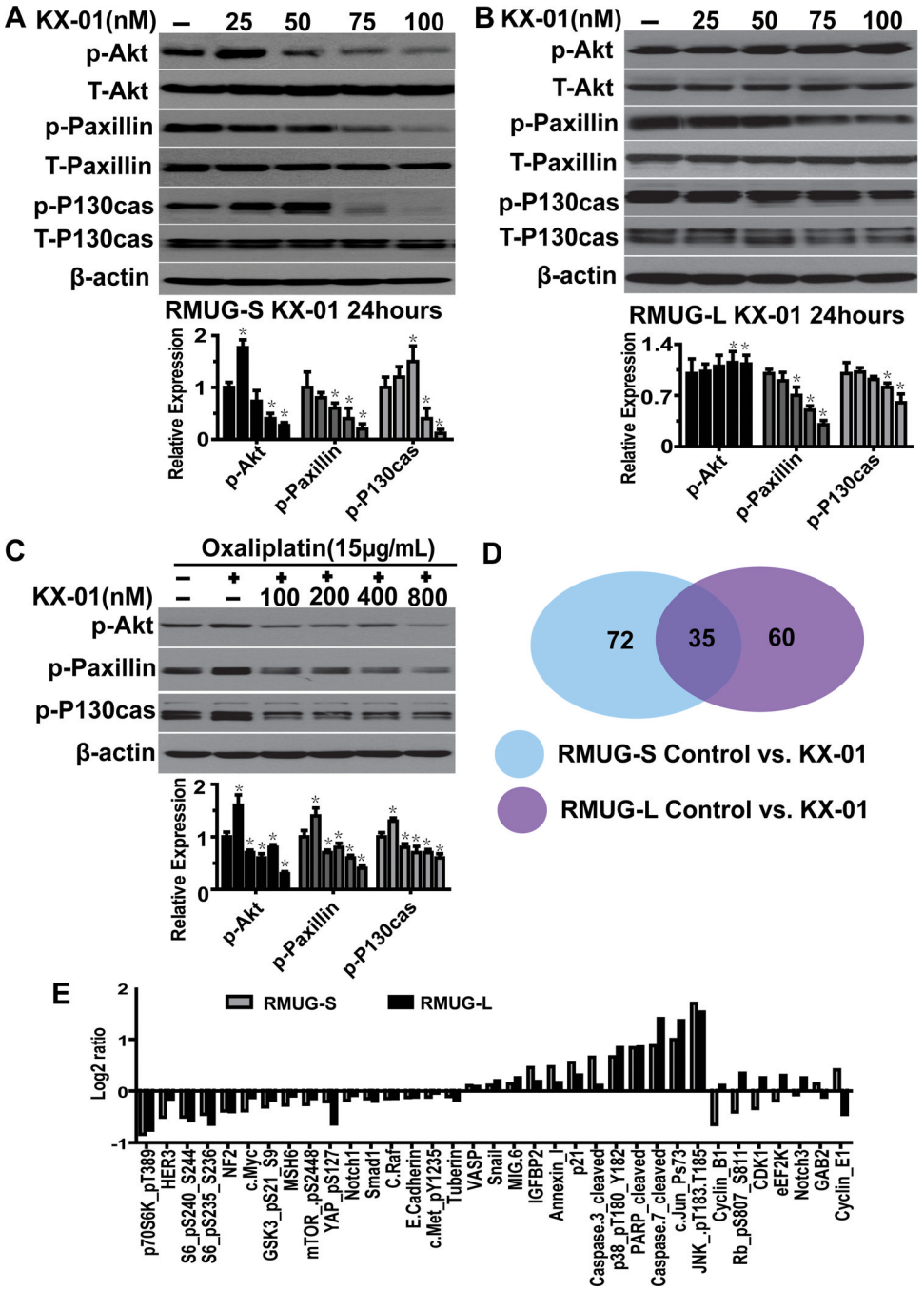

Figure 3.

Molecules involved in the mechanism of action in KX-01. (**A, B**) Western blot results showing the relative expression of Src downstream molecules (Akt, paxillin, and P130cas) in RMUG-S and RMUG-L cells treated with various concentrations of KX-01 for 24 hours. (**C**) Western blot results showing p-Akt, p-paxillin, and p-P130cas expression in cells treated with various concentrations of KX-01, followed by treatment with 15 μg/mL oxaliplatin. β-Actin was used as the loading control. Densitometry was used to calculate the ratio of each band to β-actin, normalized by control samples, each experiment was repeated three times, and bars represent means with standard errors. *p<0.05 compared with the

control group. (**D**) Venn diagram showing the number of proteins involved in the mechanism of action in KX-01 in RMUG-S and RMUG-L cells according to reverse-phase protein array analysis. (**E**) Molecules whose expression differed significantly ($p<0.05$) between cells treated with KX-01 and control cells in both RMUG-S and RMUG-L cells.

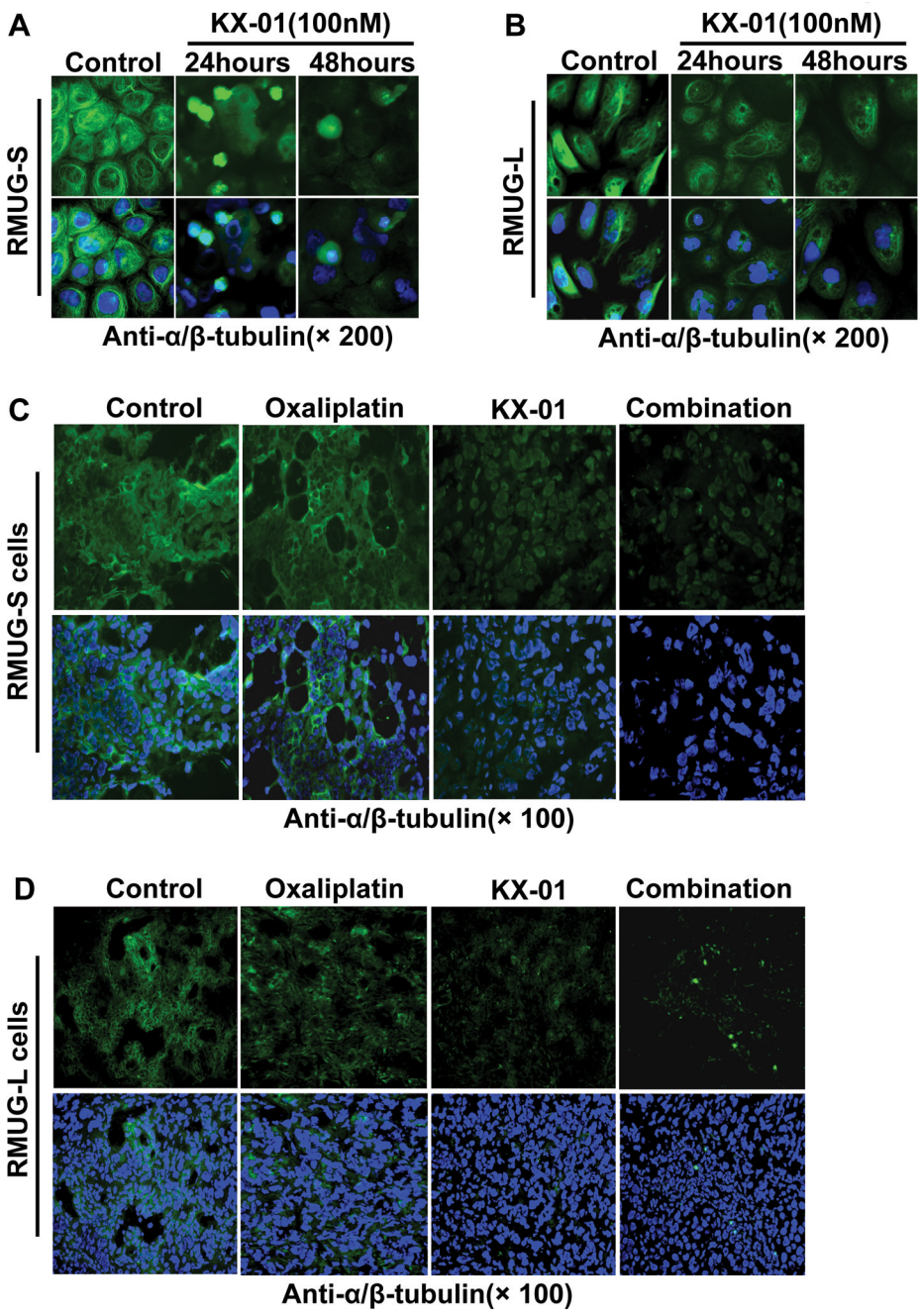

Figure 4.

The microtubule network was disrupted by KX-01. (**A, B**) α/β-tubulin immunofluorescent staining (green) in RMUG-S and RMUG-L cells treated with 100nM KX-01 for 24 or 48 hours and incubated with anti-α/β-tubulin antibody followed by Alexa Fluor 488–conjugated anti-rabbit antibody. Nuclear staining (blue) was with Hoechst 33342. Upper: tubulin stain only; Lower: tubulin and Hoechst 33342 nuclear stain. (**C, D**) α/β-tubulin immunofluorescent staining (green) in frozen tumor sections from the control, oxaliplatin, KX-01, and combination groups in the RMUG-S and RMUG-L mouse models. Nuclear staining (blue) was with Hoechst 33342. Upper: tubulin stain only; Lower: tubulin and Hoechst 33342 nuclear stain.

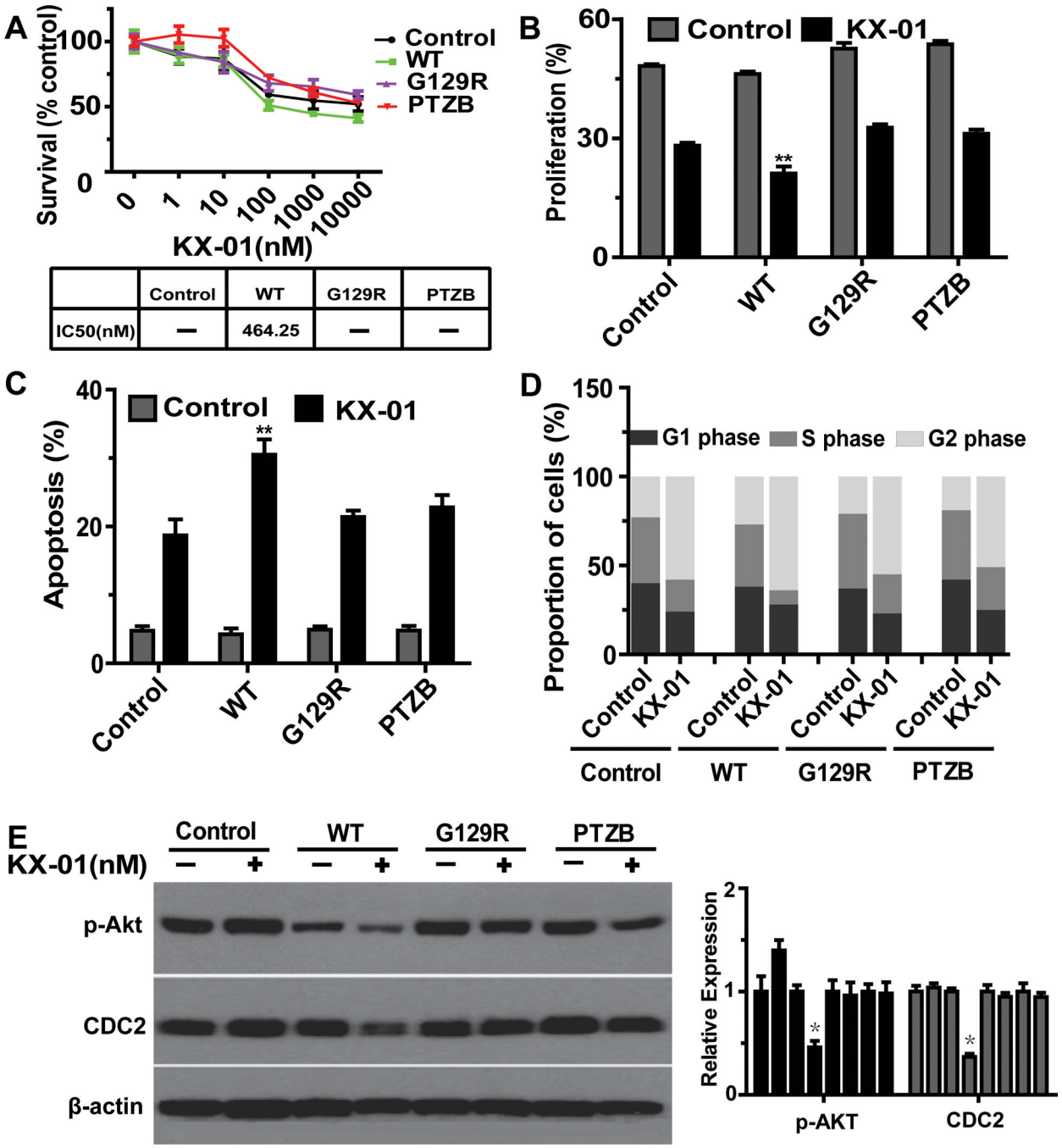

Figure 5.

PTEN deletion is involved in resistance to KX-01. (**A**) MTT assay results showing cytotoxicity of KX-01 in RMUG-L cells transfected with wild type (WT) and domain mutation (G129R, PTZB) *PTEN* and exposed to various concentration of KX-01 for 72hours. Cell survival was calculated as the number of cells surviving relative to the number of cells surviving in the control group. IC50 indicates median inhibitory rate. (**B**) EdU assay results showing inhibition of cell proliferation in cells treated with 100nM KX-01 for 72 hours. (**C**) Annexin V and 7-aminoactinomycin D assay result showing cell apoptosis in cells treated with 100nM KX-01 for 72 hours. (**D**) Flow cytometry results showing induction

of mitotic arrest in cells treated with 100nM KX-01 for 72hours. (**E**) Western blot results showing that p-Akt and CDC2 (cdk1) were inhibited in *PTEN* wild type cells. Cells were treated with 100nM KX-01 for 24 hours. β-actin was used as the loading control. All experiments were repeated at least 3 times, and bars represent means with standard errors. *$p<0.05$, **$p<0.01$ compared with control treatment (no KX-01).